ORIGINAL PAPER

Analytical Investigation on CNT Based Maxwell Nano-fluid with Cattaneo–Christov Heat Flux Due to Thermal Radiation

K. Gangadhar[1] · **K. Keziya**[1] · **T. Kannan**[2] · **Shankar Rao Munjam**[3]

Abstract

At first, we derive a series form solution of the coupled highly nonlinear equations, which includes various conditions. Then, via the method of directly defined inverse mapping with the series form solution firstly reported in this paper, we can obtain theoretical and approximate analytical analysis about the transfer of heat as well as the magnetohydrodynamic flow of Maxwell nanofluid by the influence of convective heating with effects of thermal radiation. In the energy equation, heat flux model is adopted to develop the equations for viscoelastic relaxation over boundary layer flow. For this investigation, we considered base liquid as engine oil and other forms of carbon nanotubes such as single walled nanotubes and multi-walled nanotubes. Suitable similarity transformations are applied for transformation of given boundary layer flow equations. Results are compared numerically by Keller–Box method. It is found that for both singled and multi-walled carbon nanotube based nanofluids the thermal relaxation time and temperature function are inversely proportional. More interestingly it is noted that for the two types of nanofluids, fluid relaxation parameter exactly coordinates with heat transfer rate as well as skin friction investigated. Also shown that the base functions of solutions are highly convergence.

Keywords Cattaneo–Christov heat flux · Convective heating · MDDIM · Thermal radiation · Keller–Box method

✉ Shankar Rao Munjam
munjam.shankarrao11@gmail.com

K. Gangadhar
kgangadharmaths@gmail.com

K. Keziya
keziyamathematics@gmail.com

T. Kannan
tkannanmat@gmail.com

[1] Department of Mathematics, Acharya Nagarjuna University, Ongole, AP 523001, India

[2] Department of Mathematics, School of Humanities and Sciences, SASTRA (Deemed to be University), Thanjavur, TN, India

[3] Department of Mathematics, Visvesvaraya National Institute of Technology Nagpur, South Ambazhari Road, Nagpur, Maharahashtra 440010, India

List of symbols

u', v'	Velocity components (m s^{-1})
x, y	Coordinates
$\hat{q}$	Heat flux
T_w	Wall temperature (K)
T_∞	Ambient temperature (K)
g	Gravitational force (m s^{-2})
C_p	Specific heat (J kg^{-1} K^{-1})
$\bar{V}$	Velocity vector
q_r	Radiative heat flux
k_e	Mean absorption coefficient
T	Fluid temperature
f	Nondimensional stream function
Gr_x	Grashof number
M	Magnetic parameter
Nr	Radiation parameter
Pr	Prandtl number
C_{fx}	Skin friction coefficient
Nu_x	Nusselt number
Re_x	Reynolds number

Greek symbols

λ_1	Fluid relaxation time
$\hat{\rho}$	Density (kg m^{-3})
μ'	Dynamic viscosity (N m s^{-1})
β	Thermal expansion coefficient (K^{-1})
σ	Electrical conductivity
λ_2	Thermal relaxation time
$\bar{\alpha}$	Thermal diffusivity (m^2 s^{-1})
σ_s	Stefan–Bolzmann constant
ϕ	Volume fraction of nanoparticles
$\bar{\psi}$	Stream function
η	Similarity variable
θ	Nondimensional temperature
ξ	Velocity slip factor
ζ	Thermal slip factor

Subscripts

nf	Nanofluid
f	Base fluid
w	Condition at wall
∞	Condition at infinity

Introduction

The attention on electrically conducting fluid with magnetic field is of greater importance in many applications of engineering industries such as power generation, metals purification process, hardening, MHD pumps etc. The process of cooling of stretched sheets or filaments are through a quiescent fluid and the quality and characters of the final product depends upon the rate of cooling in various processes. The cooling rate can be governed by drawing such strips or filaments into the fluid, which leads to get the final product with desired characteristics. The magnetic field can produce a significant amount of Lorentz force in the presence of a magnetization force and electric current. It is prominent that the impact of hall current is very essential in the presence of a strong magnetic field. Besides, in a low-density ionized gas the conductivity normal to the magnetic field is decreased by free growth of electrons and ions with or without magnetic field. Gupta [1] examined the impact of Hall effects of the hydromagnetic flow over flat plate. Hayat et al. [2] reported the effects of Hall current and heat transfer on the rotating flow through a porous medium. Saleem and Aziz [3] investigated the hydromagnetic flow over a stretching surface in the presence of Hall current. Aziz and Nabil [4] studied the effects of Hall current on hydromagnetic mixed convection flow past an exponentially stretching surface. Pal [5] considered thermal radiation effects on the unsteady flow of viscous fluid past a permeable stretching surface with Hall current. Gangadhar et al. [6] studied the effects of Newtonian heating about MHD flow concerning micro polar nanofluid over permeable stretching/shrinking sheet.

Nanotechnology has impacted the world of science, technology, medical sciences, engineering significantly and remarkably influencing future technologies and solutions. Suspending nano particles in the base fluid not only enhances the thermal properties of the fluids but also affects the velocity of the fluids. Researchers have been used various of models to study the different thermal and physical properties of nanofluids. One of the pioneering models are presented by Choi [7, 8] and Hamilton and Crosser model [9]. Buongiorno [10] incorporated both Brownian motion and thermophoresis in his model. The above-mentioned models focus only the spherical or rotational elliptical nature of the nanoparticles [11]. In regard to Maxwell's theory [12], Xue recommended a model that includes the rotational elliptical nanotubes and it considers large axial ratio and the space distribution on CNTs. CNTs is opening doors to many technological and industrial area that involve heat transfer, such as fast cooling of chips, ultra-capacitors, electrochemical supercapacitor, etc. [13–15].

Types of carbon nanotubes are categorized as, single-walled carbon nanotubes and multi-walled carbon nanotubes. Murshed et al. [16] found that the carbon nanotubes increase the thermal conductivity six times that of the base fluid. Ganesh Kumar et al. [17] deliberated the impact of non-linear radiation of viscoelastic nanofluid flow over elongating sheet. Khan et al. [18] analyzed about transfer of heat resolution of CNT founded nanofluids by the consequences of slip of velocity through non-parallel walls. Recently, various aspects of magnetic force, heat generation, shape effects, radiation, etc. on nanoparticles were studied by [19–59].

The analysis of heat transfer plays a very crucial role in nature and almost in all industrial sectors. The phenomena of heat transfer are clearly explained in Fourier's law of heat conduction [60]. Though, the main flaw of the Fourier's laws is the principle of causality. By employing the thermal relaxation time in the Fourier's model leads to a finite heat distribution rate [61]. Besides, Maxwell–Cattaneo model is improved significantly when time derivative is considered by Christov [62]. Tibullo and Zampoli [63] obtained uniqueness result for Cattaneo–Christov heat conduction model. Fluid flow and heat transfer with Cattaneo–Christov

124   Page 4 of 25

Int. J. Appl. Comput. Math (2020) 6:124

heat flux model is examined by Han et al. [64]. Flow of Maxwell fluid over a linear stretching sheet with the Cattaneo–Christov heat flux is reported by Mustafa [65]. The detailed discussions of the flow over a stretching sheet with variable thickness with Cattaneo–Christov heat flux model are available in the literature [66–68]. Oyelakin et al. [69] explored the Catteneo–Christov heat flux phenomenon by past nanofluid flow as well as transfer of heat resolution on vertical cone inside porous medium. Farooq et al. [70] examined the dissection of heat as well as mass flux phenomenon by Cattaneo–Christov over compressed flow contain inside porous medium along with changeable mass distribute. Prabir Kumar et al. [71] studied the influence of Cattaneo–Christov heat flux on the boundary layer flow past a stretching sheet.

In the highest degree of perception, no one at any time endeavor to investigate about MHD flow concerning CNT engine oil through non-linear enlarging surface by means of heat flux model by Cattaneo–Christov with MDDIM [72]. Outcome of convective heating as well as thermal radiations are made of use in equation of energy. The governing PDEs are transformed as extremely non-linear ODEs. Owing to non-linearly as well as outline essence of the question, an accurate resolution is different. A catalogue of counterpart co-efficient among the activity factors as well as the physical measures of observation of this model estimated to appraise the link between the flow as well as temperature are pictured through charts and graphs.

Recently, Liao [72] has been developed the new technique MDDIM and analyzed the various types of nonlinear problems. The nonlinear system of differential equations with convective heat transfer on a porous flat plate was studied by Baxter et al. [73]. After that Dewasurendra et al. [74] has been analyzed the coupled systems of nonlinear differential equations of nanofluid flow problem with mass and heat transfer effects by MDDIM.

To the best of authors' knowledge this governing equations has not been examined with MDDIM before and the reported results are new. All the obtained outcomes from the above approximate analytic and numerical procedures are displayed through graphs and tables to discuss various resulting parameters.

Mathematical Formulation

For our study we considered a two-dimensional flow which is steady, viscous and magnetohydrodynamic upper convective viscoelastic Maxwell nanofluid having both single and multi-walled carbon nanotubes on a vertical sheet. The base fluid for this investigation is viscous engine oil. In the coordinate frame y-axis is fixed along the plane and x-axis is upright to it which is shown in Fig. 1. The nanofluid moves in positive y-direction with velocity $u_w' = a'x^m$, where 'a'' indicates the constant of stretching rate and 'm' denotes the stretching index may not be an integer. The fluid flow is considered as laminar and applied magnetic field of intensity $\tilde{B}(x) = \tilde{B}_0 x^{\frac{m-1}{2}}$ is perpendicular to the sheet. Moreover, it is assumed that outward applied electric field is very small hence we have negligible magnetic Reynolds numbers. Correspondingly, it is noted that magnetic flux inside is considerably small with outward magnetic flux. There is a constant temperature T_w inside the boundary layer whereas T_∞ outside it. The equations governing the flow are given below (see Kundu et al. [71]):

$$\frac{\partial u'}{\partial x} + \frac{\partial v'}{\partial y} = 0 \tag{1}$$

$$u'\frac{\partial u'}{\partial x} + v'\frac{\partial u'}{\partial y} + \lambda_1 \left(u'^2 \frac{\partial^2 u'}{\partial x^2} + v'^2 \frac{\partial^2 u'}{\partial y^2} + 2u'v'\frac{\partial^2 u'}{\partial x \partial y} \right)$$

$$= \frac{1}{\widehat{\rho}_{nf}} \left(\mu'_{nf} \frac{\partial^2 u'}{\partial y^2} + g \left(\widehat{\rho}\beta \right)_{nf} (T - T_\infty) - \sigma \tilde{B}^2(x) u' \right) \tag{2}$$

$$\widehat{\rho} C_p \left(u' \frac{\partial u'}{\partial x} + v' \frac{\partial T}{\partial y} \right) = -\nabla \cdot \hat{q} - \frac{\partial q_r}{\partial y} \tag{3}$$

where u' is the x portion of velocity, v' is the y portion of velocity. The third term of expression (2) represents the convective part of the Maxwell fluid and λ_1 is the relaxation of the time for velocity, $\hat{q}$ is the heat flux. $\widehat{\rho}_{nf}$ is the effective density of the nanofluid, μ'_{nf} is the effective dynamic viscosity of nanofluid, β is the thermal expansion coefficient regarding to the volume, σ is the electrical conductivity, g is the gravitational force, C_p is the specific heat at constant pressure. We have,

$$\hat{q} + \lambda_2 \left[\frac{\partial \hat{q}}{\partial t} + \bar{V} \cdot \nabla \hat{q} - \hat{q} \cdot \nabla \bar{V} + \left(\nabla \cdot \bar{V} \right) \hat{q} \right] = -\tilde{K}_f \nabla T - \frac{\partial q_r}{\partial y} \tag{4}$$

Here $\bar{V}$ is the velocity vector and λ_2 is the relaxation of time of heat flux, $\tilde{K}_{nf}$ is the thermal conductivity of the nanofluid. For incompressible fluids Eq. (4) becomes

$$\hat{q} + \lambda_2 \left[\frac{\partial \hat{q}}{\partial t} + \bar{V} \cdot \nabla \hat{q} - \hat{q} \cdot \nabla \bar{V} \right] = -\tilde{K}_f \nabla T - \frac{\partial q_r}{\partial y} \tag{5}$$

Eliminating $\hat{q}$, we get:

$$u' \frac{\partial T}{\partial x} + v' \frac{\partial T}{\partial y} + \lambda_2 \left(u' \frac{\partial u'}{\partial x} \frac{\partial T}{\partial x} + v' \frac{\partial v'}{\partial y} \frac{\partial T}{\partial y} + u' \frac{\partial u'}{\partial x} \frac{\partial T}{\partial y} + v' \frac{\partial u'}{\partial y} \frac{\partial T}{\partial x} \right.$$
$$\left. + 2u'v' \frac{\partial^2 T}{\partial x \partial y} + u'^2 \frac{\partial^2 T}{\partial x^2} + v'^2 \frac{\partial^2 T}{\partial y^2} \right) = \bar{\alpha}_{nf} \frac{\partial^2 T}{\partial y^2} - \frac{\partial q_r}{\partial y} \tag{6}$$

Here $\bar{\alpha}_{nf}$ is the thermal diffusivity of the nanofluid.

The Rosseland diffusion approximation of radiation heat flux q_r is given by

$$q_r = -\frac{4\sigma_s}{3k_e} \frac{\partial T^4}{\partial y} \tag{7}$$

where σ_s is the Stefan–Bolzmann constant and k_e is the mean absorption coefficient. If the temperature differences are significantly small, then Eq. (7) can be linearized by expanding T^4 into the Taylor series about T_∞ which, after neglecting higher order terms, takes the form

$$T^4 = 4T_\infty^3 T - 3T_\infty^4 \tag{8}$$

Using Eqs. (7) and (8), Eq. (6) reduces to

$$u' \frac{\partial T}{\partial x} + v' \frac{\partial T}{\partial y} + \lambda_2 \left(u' \frac{\partial u'}{\partial x} \frac{\partial T}{\partial x} + v' \frac{\partial v'}{\partial y} \frac{\partial T}{\partial y} + u' \frac{\partial u'}{\partial x} \frac{\partial T}{\partial y} \right.$$
$$\left. + v' \frac{\partial u'}{\partial y} \frac{\partial T}{\partial x} + 2u'v' \frac{\partial^2 T}{\partial x \partial y} + u'^2 \frac{\partial^2 T}{\partial x^2} + v'^2 \frac{\partial^2 T}{\partial y^2} \right)$$
$$= \bar{\alpha}_{nf} \frac{\partial^2 T}{\partial y^2} + \frac{16\sigma_s T_\infty^3}{3k_e \rho C_p} \frac{\partial^2 T}{\partial y^2} \tag{9}$$

Maxwell's relation for thermal conductivity is

$$\bar{\alpha}_{nf} = \frac{\tilde{K}_{nf}}{\tilde{K}_f} = 1 + \frac{3 \left(\bar{\alpha}_{nf} - 1 \right) \varphi}{\left(\bar{\alpha}_{nf} + 2 \right) \left(\bar{\alpha}_{nf} - 1 \right) \varphi} \tag{10}$$

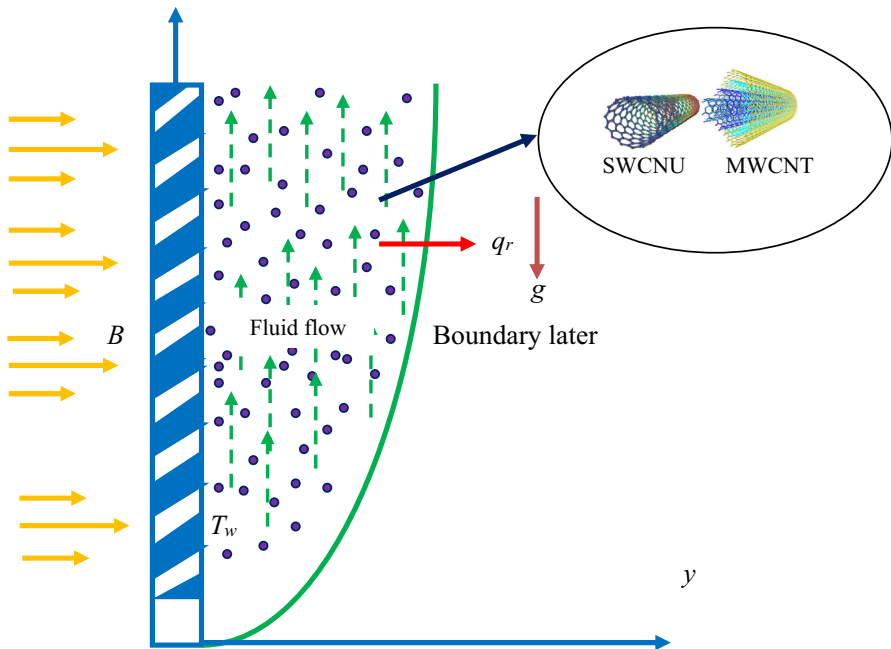Here φ is the volume fraction of nanoparticles.

Fig. 1 Flow configuration and coordinate system

Jeffery model for thermal conductivity is

$$\frac{\tilde{K}_{nf}}{\tilde{K}_f} = 1 + 3\bar{\lambda}\varphi + \left(3\bar{\lambda}^2 + \frac{3\bar{\lambda}^2}{4} + \frac{9\bar{\lambda}^3}{16}\frac{\bar{\alpha}_{nf}+2}{2\bar{\alpha}_{nf}+3} + \cdots\right)\varphi^2 \tag{11}$$

Here $\bar{\lambda} = \frac{\bar{\alpha}_{nf}-1}{\bar{\alpha}_{nf}+2}$. The results of the two models coincide when the concentration is low.

Thermal conductivity is expressed by Hamilton and Crosser model as

$$\frac{\tilde{K}_{nf}}{\tilde{K}_f} = \frac{\bar{\alpha}_{nf} + (n'-1) - (n'-1)(1-\bar{\alpha}_{nf})\varphi}{\bar{\alpha}_{nf} + (n'-1) + (1-\bar{\alpha}_{nf})\varphi} \tag{12}$$

Here n' is the shape feature of nanoparticle which is of the form of $n' = \frac{3}{\varphi^\omega}$. Where '$\omega$' takes values between 1 and 2. If $\varphi = 1$ then the shape of the nanoparticle is spherical and for $\varphi = 0.5$ it is cylindrical in shape. Xue [11] observed that these models work well when the shapes of nanoparticle either spherical or elliptical with low eccentricity also be observed that it can't explain the effect of CNTs like thermal conductivity distribution. To overcome this again Xue [11] suggested a model

$$\frac{\tilde{K}_{nf}}{\tilde{K}_f} = \frac{1 - \varphi + 2\varphi \frac{\tilde{K}_{CNT}}{\tilde{K}_{CNT}-\tilde{K}_f} \ln \frac{\tilde{K}_{CNT}+\tilde{K}_f}{2\tilde{K}_f}}{1 - \varphi + 2\varphi \frac{\tilde{K}_f}{\tilde{K}_{CNT}-\tilde{K}_f} \ln \frac{\tilde{K}_{CNT}+\tilde{K}_f}{2\tilde{K}_f}} \tag{13}$$

Here, $\tilde{K}_{CNT}$ is thermal conductivity of the CNTs. The thermo-physical characteristics of the CNT-engine oil of nanofluid are estimated with the help of the following expressions and Table 1.

Table 1 Thermo-physical properties (see Kundu et al. [71])

Physical quantity	Base fluid (viscous engine oil)	Nanoparticles (SWCNT)	Nanoparticles (MWCNT)
$\widehat{\rho}\left(\text{kg}/\text{m}^3\right)$	884	2600	1600
C_p (J/kg K)	1910	425	796
k (W/m K)	0.144	6600	3000
$\beta \times 10^{-5}$ (K^{-1})	70	2.6	2.8

The expression of dynamic viscosity of the nanofluid is given by

$$\mu'_{nf} = \frac{\mu'_f}{(1-\varphi)^{2.5}} \tag{14}$$

Here $\mu_f{}'$ is the effective viscosity of the base fluid i.e. engine oil. φ is the volume fraction of the CNTs which are both SWCNTs and MWCNTs. If $\left(\widehat{\rho}C_p\right)_{nf}$ is the effective heat capacity, then $\bar{\alpha}_{nf}$ is given by

$$\widehat{\rho}_{nf} = (1-\varphi)\widehat{\rho}_f + \varphi\widehat{\rho}_{CNT}, \quad \left(\widehat{\rho}C_p\right)_{nf} = (1-\varphi)\left(\widehat{\rho}C_p\right)_f + \varphi\left(\widehat{\rho}C_p\right)_{CNT},$$

$$\bar{\alpha}_{nf} = \frac{\tilde{K}_{nf}}{\left(\widehat{\rho}C_p\right)_{nf}}, \quad \left(\widehat{\rho}\beta\right)_{nf} = (1-\varphi)\left(\widehat{\rho}\beta\right)_f + \varphi\left(\widehat{\rho}\beta\right)_{CNT} \tag{15}$$

In the above equation $\widehat{\rho}_{CNT}$ and $\widehat{\rho}_f$ are the density of CNTs and base fluid, respectively, and $\left(\widehat{\rho}C_p\right)_{CNT}$, $\left(\widehat{\rho}C_p\right)_f$ are the heat capacity of CNTs and base fluid, respectively. β_{CNT}, β_f are the thermal expansion co-efficient of CNTs as well as base fluid.

Boundary Conditions

Boundary conditions of the above system is considered as

$$u' = u'_w + u'_s, \quad v' = 0, \quad T = \dot{T}_w + T_s, \quad \text{at} \ \ y = 0$$
$$u' \to 0, \quad T \to T_\infty, \quad \text{as} \ \ y \to \infty \tag{16}$$

$u_s{}'$ is the velocity slip which is proportional locally to the shear stress at the wall, i.e. $u'_s = \dot{l}_1 \frac{\partial u'}{\partial y}$, where $\dot{l}_1$ shows momentum slip parameter and expressed as $\dot{l}_1 = l_1 x^{-\frac{m-1}{2}}$. Furthermore, the slip temperature near solid boundary indicated as $T_s = \dot{l}_2 \frac{\partial T}{\partial y}$, and $\dot{l}_2 = l_2 x^{-\frac{m-1}{2}}$ is called as the thermal slip parameter. If no slippage case then $\dot{l}_1 = \dot{l}_2 = 0$.

Non-dimensionalization

Arrange the stream function $\bar{\psi}$ such that fulfilling the expression of continuity interpreted as $u' = \frac{\partial \bar{\psi}}{\partial y}$ as well as $v' = -\frac{\partial \bar{\psi}}{\partial x}$. Then the expressions (2), (9) and the corresponding boundary conditions (16) are modified as follows

$$
\frac{\partial \bar{\psi}}{\partial y}\frac{\partial^2 \bar{\psi}}{\partial x \partial y} - \frac{\partial \bar{\psi}}{\partial x}\frac{\partial^2 \bar{\psi}}{\partial y^2} + \lambda_1 \left(\left(\frac{\partial \bar{\psi}}{\partial y}\right)^2 \frac{\partial^3 \bar{\psi}}{\partial x^2 \partial y} + \left(\frac{\partial \bar{\psi}}{\partial x}\right)^2 \frac{\partial^3 \bar{\psi}}{\partial y^3} - 2\frac{\partial \vec{\psi}}{\partial y}\frac{\partial \bar{\psi}}{\partial x}\frac{\partial^3 \bar{\psi}}{\partial x \partial y^2} \right)
$$

$$
= \frac{1}{\left(1 - \varphi + \varphi \frac{\widehat{\rho}_{CNT}}{\widehat{\rho}_f}\right)} \left(\frac{\nu_f}{(1-\varphi)^{2.5}}\frac{\partial^3 \bar{\psi}}{\partial y^3} + \left(1 - \varphi + \varphi \frac{(\widehat{\rho}\beta)_{CNT}}{(\widehat{\rho}\beta)_f}\right)\frac{(\widehat{\rho}\beta)_f}{\widehat{\rho}_f}g(T - T_\infty) - \frac{\sigma \bar{B}^2(x)}{\widehat{\rho}_f}\frac{\partial \bar{\psi}}{\partial y} \right)
$$

$$(17)$$

$$
\frac{\partial \bar{\psi}}{\partial y}\frac{\partial T}{\partial x} - \frac{\partial \bar{\psi}}{\partial x}\frac{\partial T}{\partial y} + \lambda_2 \left(\frac{\partial \bar{\psi}}{\partial y}\frac{\partial^2 \bar{\psi}}{\partial x \partial y}\frac{\partial T}{\partial x} + \frac{\partial \bar{\psi}}{\partial x}\frac{\partial^2 \bar{\psi}}{\partial x \partial y}\frac{\partial T}{\partial y} - \frac{\partial \bar{\psi}}{\partial y}\frac{\partial^2 \bar{\psi}}{\partial x^2}\frac{\partial T}{\partial y} \right.
$$

$$
\left. - \frac{\partial \bar{\psi}}{\partial x}\frac{\partial^2 \bar{\psi}}{\partial y^2}\frac{\partial T}{\partial x} - 2\frac{\partial \bar{\psi}}{\partial y}\frac{\partial \bar{\psi}}{\partial x}\frac{\partial^2 T}{\partial x \partial y} + \left(\frac{\partial \bar{\psi}}{\partial y}\right)^2 \frac{\partial^2 T}{\partial x^2} + \left(\frac{\partial \bar{\psi}}{\partial x}\right)^2 \frac{\partial^2 T}{\partial y^2} \right)
$$

$$
= \frac{\tilde{K}_{nf}}{(1-\varphi)\left(\widehat{\rho}C_p\right)_f + \varphi\left(\widehat{\rho}C_p\right)_{CNT}}\frac{\partial^2 T}{\partial y^2} + \frac{16\sigma_s T_\infty^3}{3k_e \rho C_p}\frac{\partial^2 T}{\partial y^2}
$$

$$(18)$$

With boundary conditions

$$
\frac{\partial \bar{\psi}}{\partial y} = a'x^m + l'_2\frac{\partial^2 \bar{\psi}}{\partial y^2}, \quad \frac{\partial \bar{\psi}}{\partial x} = 0, \; T = \dot{T}_w + l'_2\frac{\partial T}{\partial y}, \; \text{at } y = 0,
$$

$$
\frac{\partial \bar{\psi}}{\partial y} \to 0, \; T \to T_\infty \text{ as } y \to \infty
$$

$$(19)$$

Furthermore, originating the local similarity transformation like

$$
\eta = y\sqrt{\frac{a'x^{m-1}}{\nu_f}}, \quad \bar{\psi} = \sqrt{a'x^{m+1}\nu'_f}\,f(\eta), \quad \theta(\eta) = \frac{T - T_\infty}{\dot{T}_w - T_\infty}
$$

$$(20)$$

Hence

$$
u' = a'x^m f'(\eta), \quad v' = -\frac{1}{2}\sqrt{a'\nu_f x^{m-1}}\{(m+1)f(\eta) + (m-1)\eta f'(\eta)\}
$$

$$(21)$$

Substitute the expression (17) into the expressions (14)–(16), we can obtain

$$
f''' + (1-\varphi)^{2.5}\left[\left(1 - \varphi + \varphi\frac{\widehat{\rho}_{CNT}}{\widehat{\rho}_f}\right)\left(\frac{m+1}{2}ff'' - mf'^2\right.\right.
$$

$$
-\alpha\left\{\begin{array}{l} m(m-1)f'^3 - \frac{m^2-1}{4}\eta f'^2 f'' \\[2mm] +\frac{(m+1)^2}{4}f^2 f''' - \frac{(m+1)(3m-1)}{2}ff'f''' \end{array}\right\}\right)
$$

$$
\left. -M^2 f' + \left(1 - \varphi + \varphi\frac{(\widehat{\rho}\beta)_{CNT}}{(\widehat{\rho}\beta)_f}\right)\bar{\lambda}\theta\right] = 0
$$

$$(22)$$

$$(1 + Nr)\frac{1}{\text{Pr}} \frac{\tilde{K}_{nf}}{\tilde{K}_f} \theta'' + \left\{ 1 - \varphi + \varphi \frac{(\hat{\rho} C_p)_{CNT}}{(\hat{\rho} C_p)_f} \right.$$

$$\left. \times \left[\begin{array}{c} \frac{m+1}{2} f\theta' - 2mf'\theta - \gamma \\ \left[\begin{array}{c} (6m^2 - 2m)\theta f' + \frac{(3-9m)(m+1)}{4} ff'\theta' \\ -m(m+1)\theta f f'' + \frac{(m+1)^2}{4} f^2 \theta'' \end{array} \right] \end{array} \right] \right\} = 0 \tag{23}$$

The appropriate boundary conditions are

$$f(0) = 0, \quad f'(0) = 1 + \xi f''(0), \quad \theta(0) = 1 + \zeta \theta'(0), \quad \text{at } \eta = 0$$
$$f'(\eta) = 0, \quad \theta(\eta) = 0, \quad \text{as } \eta \to \infty \tag{24}$$

In the above equations η represents similarity variable; $f(\eta)$ denotes the non-dimensional stream function; $\theta(\eta)$ denotes the non-dimensional temperature; $\bar{\lambda} = \frac{Gr_x}{\text{Re}_x^2}$ denotes thermal buoyancy factor that is proportion of local Reynolds number as well as local Grashof number explicated with $\text{Re}_x = \frac{u'_w}{v'_f}$, $Gr_x = \frac{(\hat{\rho}\beta)_f (\dot{T}_w - T_\infty)x^3}{\bar{v}_f^2 \hat{\rho}_f}$ respectively. $M = \tilde{B}_0 \sqrt{\frac{\sigma}{a\hat{\rho}_f}}$ is the external magnetic flux factor. When $\bar{\lambda}$ greater than zero it supports the flow and for less than zero it obstruct the flow.

If $\bar{\lambda}$ is equal to zero it express position of forced convection. If $\bar{\lambda}$ is very much larger than 1, the force of buoyancy will be prevalent. Therefore, mixed convective flow procreates when $\bar{\lambda} = 0(1)$; $\bar{\alpha} = \bar{\lambda}_1 a'x^{m-1}$ and $\gamma = \bar{\lambda}_2 a'x^{m-1}$ illustrates fluid relaxation duration as well as thermal relaxation duration respectively. $\text{Pr} = \frac{\mu'_f (\hat{\rho} C_p)_f}{\hat{\rho}_f \tilde{K}_f}$ is the Prandtl number. Furthermore, the slip momentum factor is designated by $\xi = l_1 \sqrt{\frac{a'}{v_f}}$ and thermal slip factor is denoted as $\zeta = l_2 \sqrt{\frac{a'}{v_f}}$, $Nr = \frac{16\sigma_e T_\infty^3}{3k_e k}$ is the radiation parameter.

Physical Quantities of Interest

Physical quantities assign in current research are co-efficient of skin friction C_{fx} and the Nusselt number Nu_x are expressed as

$$C_{fx} = \frac{\mu'_{nf}}{\hat{\rho}_f \bar{u}_w^2} \left(\frac{\partial u}{\partial y} \right)_{y=0} = \frac{1}{(1-\varphi)^{2.5}} \text{Re}_x^{-\frac{1}{2}} f''(0) \tag{25}$$

$$Nu_x = -\frac{x\tilde{K}_{nf}}{\tilde{K}_f (T_w - T_\infty)} \left(\frac{\partial T}{\partial y} \right)_{y=0} + q_{ry=0} = -\text{Re}_x^{-\frac{1}{2}} \frac{\tilde{K}_{nf}}{\tilde{K}_f} (1 + Nr)\theta''(0) \tag{26}$$

Now, degraded skin friction as well as degraded Nusselt number will be defined as

$$C_{fx} = C_{fx} \text{Re}_x^{\frac{1}{2}} = \frac{1}{(1-\varphi)^{2.5}} f''(0) \tag{27}$$

$$Nu_x = Nu_x \text{Re}_x^{-\frac{1}{2}} = -\frac{\tilde{K}_{nf}}{\tilde{K}_f} (1 + Nr)\theta'(0) \tag{28}$$

Numerical Experiment

Put

$$B_1 = (1 - \varphi)^{2.5}, \quad B_2 = \left(1 - \varphi + \varphi \frac{\widehat{\rho}_{CNT}}{\widehat{\rho}_f}\right), \quad B_3 = \left(1 - \varphi + \varphi \frac{(\widehat{\rho}\beta)_{CNT}}{(\widehat{\rho}\beta)_f}\right),$$

$$B_4 = (1 + Nr)\frac{1}{Pr}\frac{\tilde{K}_n f}{\tilde{K}_f}, \quad B_5 = \left(1 - \chi + \chi \frac{(\widehat{\rho}C_p)_{CNT}}{(\widehat{\rho}C_p)_f}\right).$$

$$n_1 = \frac{m+1}{2}, \quad n_2 = m(m-1), \quad n_3 = \frac{m^2-1}{4}, \quad n_4 = \frac{(m+1)^2}{2},$$

$$n_5 = \frac{(m+1)(3m-1)}{2}, \quad n_6 = 6m^2 - 2m, \quad n_7 = \frac{(3-9m)(m+1)}{4}.$$

Now Eqs. (19)–(20) become,

$$f''' + B_1(B_2 n_1 f f'' - m f'^2 - \bar{\alpha}\{n_2 f'^3 - n_3 \eta f'^2 f''$$
$$+ n_4 f^2 f''' - n_5 f f' f''\}) - M f' + B_3 \bar{\lambda}\theta = 0 \tag{29}$$

$$B_4 \theta'' + B_5\{n_1 f \theta' - 2m f'\theta - \gamma(n_6 \theta f' + n_7 f f'\theta' - n_8 \theta f f'' + n_4 f^2 \theta'')\} = 0 \tag{30}$$

Again put

$$f' = q, \quad f'' = q' = r, \quad f''' = r' = s; \quad \theta' = p, \quad \theta'' = p'.$$

Now the Eqs. (26)–(27) will become

$$r' + B_1(B_2 n_1 fr - mq^2 - \bar{\alpha}\{n_2 q^3 - n_3 \eta q^2 r + n_4 f^2 s - n_5 f q r\} - Mq + B_3 \bar{\lambda}\theta) = 0 \tag{31}$$

$$B_4 p' + B_4[n_1 fp - 2mq\theta - r(n_6 \theta q + n_7 f q P - n_8 \theta fr + n_4 f^2 p')] = 0 \tag{32}$$

$$f_j^i - f_{j-1}^i = \frac{h_j}{2}(q_j + q_{j-1}) \tag{33}$$

$$q_j^i - q_{j-1}^i = \frac{h_j}{2}(r_j + r_{j-1}) \tag{34}$$

$$\theta_j^i - \theta_{j-1}^i = \frac{h_j}{2}(p_j + p_{j-1}) \tag{35}$$

$$\left(r_j^i - r_{j-1}^i\right) + B_1 h_j\left[B_2 n_1 f_{j-\frac{1}{2}}^i r_{j-\frac{1}{2}}^i - m\left(q_{j-\frac{1}{2}}^i\right)^2 - \bar{\alpha}\left\{n_2\left(q_{j-\frac{1}{2}}^i\right)^3\right.\right.$$

$$\left.\left. - n_3 \eta\left(q_{j-\frac{1}{2}}^i\right)^2\left(r_{j-\frac{1}{2}}^i\right) + n_4\left(f_{j-\frac{1}{2}}^i\right)^2\left(s_{j-\frac{1}{2}}^i\right) - n_5 f_{j-\frac{1}{2}}^i q_{j-\frac{1}{2}}^i r_{j-\frac{1}{2}}^i\right\}\right]$$

$$- M\left(q_{j-\frac{1}{2}}^i\right) + B_3 \bar{\lambda}\left(\theta_{j-\frac{1}{2}}^i\right) = M_{j-\frac{1}{2}} \tag{36}$$

$$B_4\left(P_j^i - P_{j-\frac{1}{2}}^i\right) + B_5 h_j\left[n_1 f_{j-\frac{1}{2}}^i P_{j-\frac{1}{2}}^i - 2m\left(q_{j-\frac{1}{2}}^i \theta_{j-\frac{1}{2}}^i\right)\right.$$

$$\left. - r\left\{n_6 \theta_{j-\frac{1}{2}}^i q_{j-\frac{1}{2}}^i + n_7 f_{j-\frac{1}{2}}^i q_{j-\frac{1}{2}}^i P_{j-\frac{1}{2}}^i - n_8 \theta_{j-\frac{1}{2}}^i f_{j-\frac{1}{2}}^i r_{j-\frac{1}{2}}^i + n_4\left(f_{j-\frac{1}{2}}^i\right)^2\right\}\right]$$

$$\frac{\left(p_j^i - p_{j-\frac{1}{2}}^i\right)}{h_j} = L_{j-\frac{1}{2}} \tag{37}$$

Here

$$M_{j-\frac{1}{2}} = -\left(r_j^{i-1} - r_{j-1}^{i-1}\right) + B_1 h_j \left[B_2 n_2 \left(f_{j-\frac{1}{2}}^{i-1} r_{j-\frac{1}{2}}^{i-1} \right) - m \left(q_{j-\frac{1}{2}}^{i-1} \right)^2 \right.$$

$$- \bar{\alpha} \left\{ n_2 \left(q_{j-\frac{1}{2}}^{i-1} \right)^3 - n_3 \eta \left(q_{j-\frac{1}{2}}^{i-1} \right)^2 r_{j-\frac{1}{2}}^{i-1} + n_4 \left(f_{j-\frac{1}{2}}^{i-1} \right)^2 s_{j-\frac{1}{2}}^{i-1} \right.$$

$$\left. \left. -n_5 f_{j-\frac{1}{2}}^{i-1} q_{j-\frac{1}{2}}^{i-1} r_{j-\frac{1}{2}}^{i-1} \right\} \right] - M q_{j-\frac{1}{2}}^{i-1} + B_3 \bar{\lambda} \theta_{j-\frac{1}{2}}^{i-1} \tag{38}$$

$$L_{j-\frac{1}{2}} = -B_4 \left(p_j^{i-1} - p_{j-1}^{i-1} \right) - B_5 h_j \left[n_1 f_{j-\frac{1}{2}}^{i-1} p_{j-\frac{1}{2}}^{i-1} - 2m \left(q_{j-\frac{1}{2}}^{i-1} \theta_{j-\frac{1}{2}}^{i-1} \right) \right.$$

$$+ r \left\{ n_6 \left(q_{j-\frac{1}{2}}^{i-1} \theta_{j-\frac{1}{2}}^{i-1} \right)^3 + n_7 f_{j-\frac{1}{2}}^{i-1} q_{j-\frac{1}{2}}^{i-1} p_{j-\frac{1}{2}}^{i-1} \right.$$

$$\left. \left. - n_5 \theta_{j-\frac{1}{2}}^{i-1} f_{j-\frac{1}{2}}^{i-1} r_{j-\frac{1}{2}}^{i-1} + n_4 \left(f_{j-\frac{1}{2}}^{i-1} \right)^2 \left(\frac{p_j^{i-1} - p_{j-1}^{i-1}}{h_j} \right) \right\} \right] \tag{39}$$

$$e_1 \delta r_j + e_2 \delta r_{j-1} + e_3 \delta q_j + e_4 \delta q_{j-1} + e_5 \delta f_j + e_6 \delta f_{j-1} = (b_5)_j \tag{40}$$

$$(e_1)_j = 1 + \frac{B_1 B_2 h_j n_1}{2} f_{j-\frac{1}{2}}^i - \frac{B_1 h_j}{2} \left(q_{j-\frac{1}{2}}^i \right)^2 \bar{\alpha} n_3 \eta \tag{41}$$

$$(e_2)_j = -1 + \frac{B_1 B_2 h_j n_1}{2} f_{j-\frac{1}{2}}^i - \frac{B_1 h_j}{2} \left(q_{j-\frac{1}{2}}^i \right)^2 \bar{\alpha} n_3 \eta \tag{42}$$

$$(e_3)_j = \frac{B_1 h_j m}{2} q_{j-\frac{1}{2}}^i - \frac{B_1 h_j \bar{\alpha} n_2}{2} \left(q_{j-\frac{1}{2}}^i \right)^2 + \frac{B_1 h_j n_3 \bar{\alpha} \eta}{2} \left(q_{j-\frac{1}{2}}^i \right) \left(r_{j-\frac{1}{2}}^i \right)$$

$$+ \frac{B_1 h_j \bar{\alpha} n_5 f_{j-\frac{1}{2}}^i r_{j-\frac{1}{2}}^i}{2} - M$$

$$(e_4)_j = (e_3)_j \tag{43}$$

$$(e_5)_j = 1 + \frac{B_1 h_j n_1}{2} r_{j-\frac{1}{2}}^i - \frac{B_1 h_j}{2} \bar{\alpha} n_4 \eta f_{j-\frac{1}{2}}^i s_{j-\frac{1}{2}}^i, \tag{44}$$

$$(e_6)_j = (e_5)_j; \tag{45}$$

$$\left(\delta f_j - \delta f_{j-1} \right) - \frac{h_j}{2} \left(q_j + q_{j-1} \right) = (b_1)_j \tag{46}$$

$$\left(\delta q_j - \delta q_{j-1} \right) - \frac{h_j}{2} \left(r_j + r_{j-1} \right) = (b_2)_j \tag{47}$$

$$\left(\delta r_j - \delta r_{j-1} \right) - \frac{h_j}{2} \left(s_j + s_{j-1} \right) = (b_3)_j \tag{48}$$

$$\left(\delta \theta_j - \delta \theta_{j-1} \right) - \frac{h_j}{2} \left(p_j + p_{j-1} \right) = (b_4)_j \tag{49}$$

$$(g_1)_j = B_4 + \frac{B_5 h_j n_1}{2} f_{j-\frac{1}{2}}^i + \frac{B_5 h_j \gamma n_7}{2} f_{j-\frac{1}{2}}^i q_{j-\frac{1}{2}}^i - B_5 \gamma n_4 \left(f_{j-\frac{1}{2}}^i \right)^2 \tag{50}$$

$$(g_2)_j = -B_4 + \frac{B_5 h_j n_1}{2} f_{j-\frac{1}{2}}^i + \frac{B_5 h_j \gamma n_7}{2} f_{j-\frac{1}{2}}^i q_{j-\frac{1}{2}}^i - B_5 \gamma n_4 \left(f_{j-\frac{1}{2}}^i \right)^2 \tag{51}$$

$$(g_3)_j = -m B_5 h_j \theta_{j-\frac{1}{2}} - \frac{B_5 h_j \gamma n_6}{2} \theta_{j-\frac{1}{2}} - B_5 h_j \gamma n_7 f_{j-\frac{1}{2}}^i p_{j-\frac{1}{2}}^i \tag{52}$$

$$(g_4)_j = (g_3)_j \tag{53}$$

$$(g_5)_j = \frac{B_5 h_j n_1}{2} p^i_{j-\frac{1}{2}} - \frac{B_5 h_j \gamma n_7}{2} q^i_{j-\frac{1}{2}} p^i_{j-\frac{1}{2}}$$
$$+ \frac{B_5 h_j n_8 \gamma}{2} \theta^i_{j-\frac{1}{2}} r^i_{j-\frac{1}{2}} + \frac{B_5 h_j n_4}{2} f^i_{j-\frac{1}{2}} \left(p^i_{j-\frac{1}{2}} \right) \tag{54}$$

$$(g_6)_j = (g_5)_j \tag{55}$$

$$(b_5)_j = B_1 h_j n_4 \left(f^i_{j-\frac{1}{2}} \right)^2 \left(s^i_{j-\frac{1}{2}} \right) + B_1 h_j n_2 \bar{\alpha} \left(q^i_{j-\frac{1}{2}} \right)^3$$
$$+ B_3 \bar{\lambda} \theta^i_{j-\frac{1}{2}} + M_{j-\frac{1}{2}} \tag{56}$$

$$(b_6)_j = B_5 h_j n_8 \theta_{j-\frac{1}{2}} f_{j-\frac{1}{2}} r_{j-\frac{1}{2}} + L_{j-\frac{1}{2}} \tag{57}$$

$$A\delta = B \tag{58}$$

where,

$$A = \begin{bmatrix} E_1 & C_1 & \cdots & \cdots & \cdots & \cdots \\ D_1 & E_2 & \cdots & \cdots & \cdots & \cdots \\ \cdots & \cdots & \cdots & \cdots & \cdots & \cdots \\ \cdots & \cdots & \cdots & \cdots & \cdots & \cdots \\ \cdots & \cdots & \cdots & \cdots & \cdots & \cdots \\ \cdots & \cdots & \cdots & \cdots & D_J & E_J \end{bmatrix} \quad \delta = \begin{bmatrix} \delta_1 \\ \delta_2 \\ \vdots \\ \vdots \\ \delta_J \end{bmatrix} \quad B = \begin{bmatrix} b_1 \\ b_2 \\ \vdots \\ \vdots \\ b_j \end{bmatrix}$$

$$E_1 = \begin{bmatrix} 0 & 0 & 1 & 0 & 0 \\ \frac{-h_1}{2} & 0 & 0 & \frac{-h_1}{2} & 0 \\ 0 & \frac{-h_1}{2} & 0 & 0 & \frac{-h_1}{2} \\ e_2 & 0 & e_5 & e_1 & 0 \\ 0 & g_2 & g_5 & 0 & g_1 \end{bmatrix} \tag{59}$$

$$C = \begin{bmatrix} \frac{-h_1}{2} & 0 & 0 & 0 & 0 \\ 1 & 0 & 0 & 0 & 0 \\ 0 & 1 & 0 & 0 & 0 \\ e_3 & 0 & 0 & 0 & 0 \\ g_3 & 0 & 0 & 0 & 0 \end{bmatrix} \tag{60}$$

$$D = \begin{bmatrix} 0 & 0 & -1 & 0 & 0 \\ 0 & 0 & 0 & \frac{-h_2}{2} & 0 \\ 0 & 0 & 0 & 0 & \frac{-h_2}{2} \\ 0 & 0 & e_6 & e_2 & 0 \\ 0 & 0 & g_6 & 0 & g_2 \end{bmatrix} \tag{61}$$

$$E_2 = \begin{bmatrix} \frac{-h_2}{2} & 0 & 1 & 0 & 0 \\ -1 & 0 & 0 & \frac{-h_2}{2} & 0 \\ 0 & -1 & 0 & 0 & \frac{-h_2}{2} \\ e_4 & 0 & e_5 & e_1 & 0 \\ g_4 & 0 & g_5 & 0 & g_1 \end{bmatrix} \tag{62}$$

The method used to solve (58) is the block elimination tri-diagonal method. The convergence criterion is set as 0.0001.

Solution of the Problem by MDDIM

For more details of MDDIM, Liao [72] was introduced this technique for finding an approximate analytical solution to highly nonlinear differential equations. The method of MDDIM is used for obtaining the approximate analytical solution of (22)–(23) with (24). We assume the set of an infinite number of base functions that are linearly independent variables areas;

$$M_\infty = \left\{ 1, \, e^{-\eta\delta}, \, e^{-2\eta\delta}, \, e^{-3\eta\delta}, \ldots \right\}. \tag{63}$$

We have considered the base functions as;

$$X = \sum_{j=0}^{\infty} \left\{ \sigma_j e^{-j\eta\delta} / \sigma_j \varepsilon \Re \right\}. \tag{64}$$

Here X is the solution and base space for $f(\eta)$ and $\theta(\eta)$.

Consider first two terms of M_∞ as

$$M_2 = \left\{ 1, \, e^{-\eta\delta} \right\}. \tag{65}$$

Next, form the space of functions taking their linear combinations

$$M* = \left\{ \sigma_0 + \sigma_1 e^{-\eta\delta} / \sigma_0, \, \sigma_1 \varepsilon \, \Re \right\}. \tag{66}$$

Take primary solutions as $\xi(\eta)$ belongs to M^* have the following form

$$\xi(\eta) = \sum_{j=0}^{1} \left\{ \sigma_j e^{-\eta\delta} \right\}. \tag{67}$$

Write,

$$\hat{A} = \left\{ e^{-2\eta\delta}, \, e^{-3\eta\delta}, \, \ldots \right\}, \tag{68}$$

and we define $\hat{X}$ as follows:

$$\hat{X} = \sum_{j=2}^{\infty} \left\{ \sigma_j e^{-j\eta\delta} / \sigma_j \varepsilon \Re \right\}. \tag{69}$$

Therefore, we get the functions as: $X = \hat{X} U M^*$.

Define base function as

$$M_R = \{ \mu_1(\eta), \, \mu_2(\eta), \, \mu_3(\eta), \ldots \} \tag{70}$$

The linear combinations of base function from Eq. (6), we defined as;

$$S = \sum_{j=1}^{\infty} \left\{ a_j \mu_j(\eta) / a_j \varepsilon \Re \right\}. \tag{71}$$

Define inversely defined mapping for the solution of f as follows;

$$\text{Define } J : S \rightarrow X \text{ by } J\left[e^{-j\eta\delta} \right] = \frac{e^{-j\eta\delta}}{Aj^3 + j}. \tag{72}$$

where δ and A, are parameters.

Define inversely defined mapping for the solution of θ as follows;

$$\text{Define } J : S \rightarrow X \text{ by } J\left[e^{-j\eta\delta} \right] = \frac{e^{-j\eta\delta}}{Aj + j}. \tag{73}$$

Table 2 Comparison of MDDIM and KBM results with that of Li et al. [68] at $f''(0)$ and $-\theta'(0)$ for various ξ and λ with $m = 0.1$, $\bar{\alpha} = 0.4$, $\gamma = 0.3$, $M = 3.0$, $Pr = 1.0$, $Nr = 0$, $Bi \to \infty$

ξ	λ	Li et al. [68]		KBM results		MDDIM results	
		$f''(0)$	$-\theta'(0)$	$f''(0)$	$-\theta'(0)$	$f''(0)$	$-\theta'(0)$
0	0.1	-1.7449	0.3910	-1.744901	0.391010	-1.744901	0.391011
	0.7	-1.4727	0.4405	-1.472675	0.440508	-1.472675	0.440507
	1.5	-1.1287	0.4901	-1.128720	0.490069	-1.128721	0.490069
	2.0	-0.9215	0.5154	-0.921465	0.515353	-0.921465	0.515353
0.5	0.1	-0.9117	0.2942	-0.911567	0.294150	-0.911567	0.294150
	0.7	-0.7639	0.3667	-0.763912	0.366735	-0.763912	0.366735
	1.5	-0.5809	0.4386	-0.580890	0.438624	-0.580890	0.438624
	2.0	-0.4722	0.4753	-0.472235	0.475267	-0.472235	0.475267

In the present problem, analysis of MDDIM, from Eq. (24), we choose the initial guesses as follows;

$$f_0(\eta) = \xi\left(1 - e^{-\eta}\right) + \eta, \quad \text{and} \quad \theta_0(\eta) = (1 - \xi)e^{-\eta}. \tag{74}$$

The objective of the proposed analysis that is MDDIM is that choosing appropriate initial profiles which sustaining the initial conditions of the current study; choose directly defined inverse mappings for the solutions, which simplifies the evaluation process analytically. From the governing equations of the present study we can write the nonlinear operator directly. In MDDIM process, we obtain a set of nonlinear differential equations which are called deformation equations and these have to solve. We assumed the set of base functions, initial guesses and directly defined inverse mappings for the solution analysis. Using computational software's MAPLE and MATHEMATICA, the governing equations are reformulated, and the series solutions computed. Since the MDDIM is explained in detail in [72–74], the method of solution procedure not presented here for the sake of brevity.

Verification of Code

An analogy in sketch among current results with that of Li et al. [68], to demonstrate preciseness of the method we executed. Table 2 displayed the determine values of co- efficient of skin friction $f''(0)$, as well as Nusselt number $\theta'(0)$, for dissimilar values of ξ and λ in non-existence of single walled as well as multi walled carbon nano tubes concentration ($\varphi = 0$) along thermal radiation ($Nr = 0$), convective heating as well ($Bi \to \infty$). Every one comfortably authenticates out of Table 2, that the data explained analytically and numerically acquired by the current techniques and that of Li et al. [68] are in excellent concord accordingly support the employ of the current code owing to present model.

Results and Discussion

In the present part, the foremost aim is to examine the transformation of temperature, non-dimensional velocity, coefficient of skin friction, and Nusselt number, by the impact of
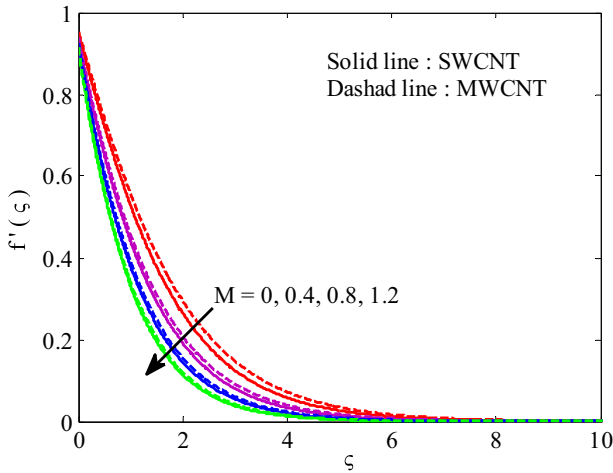
Fig. 2 The MDDIM solutions of dimensionless velocity distribution $f'(\varsigma)$ for different values of M
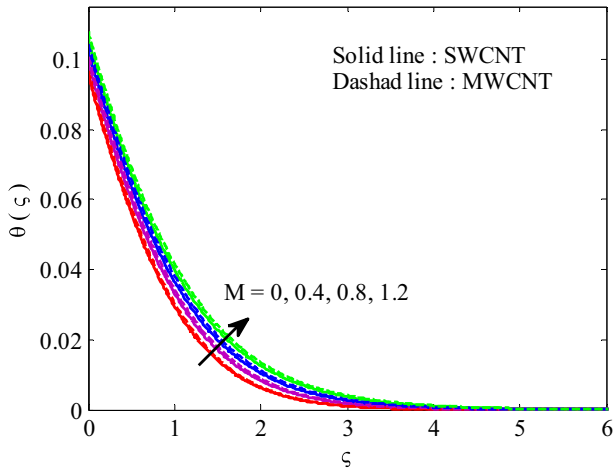

Fig. 3 The MDDIM solutions of dimensionless temperature distribution $\theta(\varsigma)$ for different values of M

changeable factors through MDDIM and KBM. Approximate analytical results and Numerical computations outcomes are shown in the Tables 2 and 3 and graphically presented in Figs. 2, 3, 4, 5, 6, 7, 8, 9, 10, 11 and 12 to discuss various resulting parameters which are involved the problem. This comparison shows a decent agreement between present approximate analytical results and previous published work. Furthermore, the outcomes demonstrate that the MDDIM and KBM are very efficient and adequately powerful for use of solving fluid flow problems. Physical and thermal characteristics of base fluid are displayed in Table 1. These characteristics are accustomed to investigate the developments appearing in temperature and velocity profiles exposed to fluctuation in dissimilar factors. To carry out the computerized imitation, the fundamental measures of the factors are cautiously calculated as $\bar{\alpha} = 0.5$, $\varphi = 0.2$, $M = 0.5$, $\bar{\lambda} = 0.1$, $m = 0.1$, $\gamma = 0.2$, $Pr = 0.7$, $B_i = 0.1$, $\xi = 0.1$, and $N_r = 0.5$ except particularize.

Table 3 Effects of different parameters on C_{fx} and Nu_x when $Pr=0.7$, $Bi=0.1$, $\lambda=0.1$ and $m=0.1$ by MDDIM

α	M	γ	ξ	χ	Nr	$C_{fx}(SWCNT)$	$Nu_x(SWCNT)$	$C_{fx}(MWCNT)$	$Nu_x(MWCNT)$
0	0.1	0.1	0.5	0.05	0.5	0.493884	0.040189	0.486581	0.041772
0.1						0.494895	0.040171	0.487670	0.041752
0.2						0.495904	0.040153	0.488757	0.041732
0.3						0.496912	0.040135	0.489842	0.041712
0.4						0.497919	0.040116	0.490925	0.041692
0.5						0.498923	0.040098	0.492005	0.041671
0.1	0.0					0.445435	0.040488	0.436648	0.042096
	0.1					0.494895	0.040171	0.487670	0.041752
	0.2					0.538205	0.039861	0.532121	0.041416
	0.3					0.576589	0.039558	0.571358	0.041088
	0.4					0.610990	0.039263	0.606417	0.040769
	0.5					0.642129	0.038975	0.638075	0.040459
	0.1	0.0				0.494984	0.040265	0.487763	0.041851
		0.1				0.494895	0.040171	0.487670	0.041752
		0.2				0.494803	0.040074	0.487576	0.041650
		0.3				0.494710	0.039975	0.487480	0.041546
		0.4				0.494614	0.039873	0.487381	0.041439
		0.5				0.494517	0.039768	0.487281	0.041328
		0.1	0.0			0.717090	0.040983	0.701879	0.042594
			0.2			0.604752	0.040620	0.594000	0.042218
			0.4			0.526194	0.040311	0.518044	0.041897
			0.6			0.467484	0.040040	0.461020	0.041616
			0.8			0.421610	0.039797	0.416317	0.041363
			1.0			0.384598	0.039578	0.380157	0.041135
			0.5	0.01		0.445469	0.064017	0.443970	0.064786
				0.05		0.494895	0.040171	0.487670	0.041752
				0.1		0.557709	0.026727	0.542684	0.028202
				0.15		0.627301	0.019504	0.603193	0.020747
				0.2		0.706962	0.014980	0.672120	0.016015
				0.05	0	0.498646	0.041817	0.491525	0.043483
					0.4	0.495644	0.040477	0.488440	0.042073
					0.8	0.492663	0.039310	0.485383	0.040849
					1.2	0.489760	0.038274	0.482416	0.039763
					1.6	0.486984	0.037347	0.479585	0.038792
					2.0	0.484362	0.036511	0.476917	0.037918

From Table 2, it is noticed that for SWCNT and MWCNT nanofluids deviations in the co-efficient of skin friction and local Nusselt number for different factors. Table 3 declare that if 'M' rises from 0 to 0.5 significantly improve the values of C_{fx} for SWCNT nano fluid is increased by 46% and MWCNT nanofluid decreased by 3.89% additionally almost equal changes in measures of M, Nu_x, is raised by 44% for SWCNT nanofluid and decreased by 3.73% for MWCNT nanofluid. The relaxation factor α of the fluid changes between 0.0
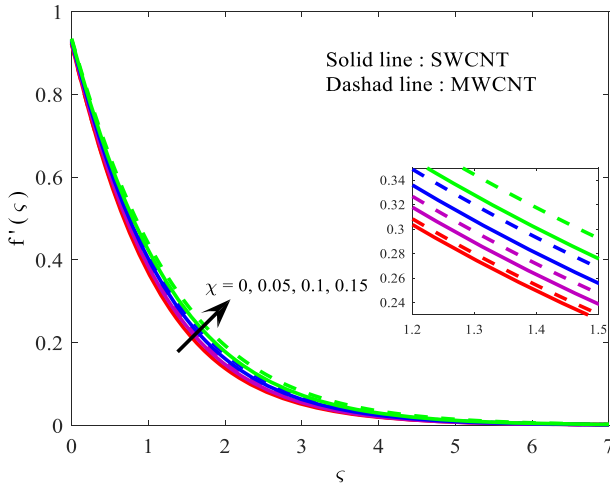
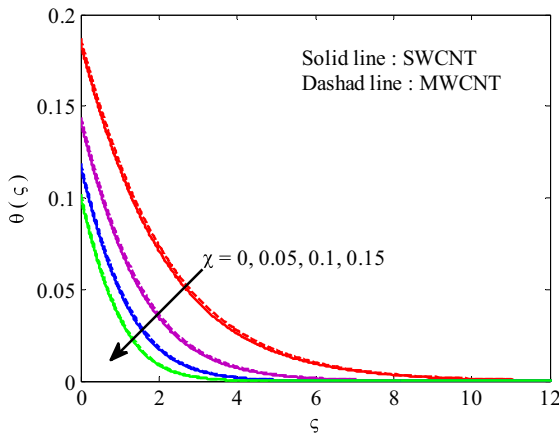**Fig. 4** The MDDIM solutions of dimensionless velocity distribution $f'(\varsigma)$ for different values of χ

Fig. 5 The MDDIM solutions of dimensionless temperature distribution $\theta(\varsigma)$ for different values of χ

and 0.5 the cut down C_{fx} and Nu_x for SWCNT is magnified by 1.02% and 1.11%, but the corresponding order of $\bar{\alpha}$, the enlargement of skin friction as well as the heat transport rate is decreased by 0.23% and 2.26% for MWCNT nanofluids. Get out of Table 3, it points that γ acquires from 0.0 to 0.5; C_{fx} procure highly less fall of 0.09% and 1.25% concerning SWCNT as well as MWCNT founded nanofluids. That means friction among the layers of solid as well as fluid hike up as a result the velocity falling off. Furthermore it is acknowledged out of Table 3 that by the identical enlargement of γ, Nu_x against SWCNT nanofluid subsided by and concerning MWCNT nano fluid is declined by 0.03% and 1.23%. Ascertained that ξ ranks out of 0.0–1.0, the co-efficient of skin friction against SWCNT as well as MWCNT founded nano fluid declined through 45% and 3.43% respectively. Merely Nu_x for the equivalent cut down through 46% and 1.21%.

A crucial remark established in Table 3 is such as φ ranks concerning 0.01–0.2, C_{fx} against SWCNT as well as MWCNT nano fluid reduced through 51.4% and 75.3%. Furthermore,
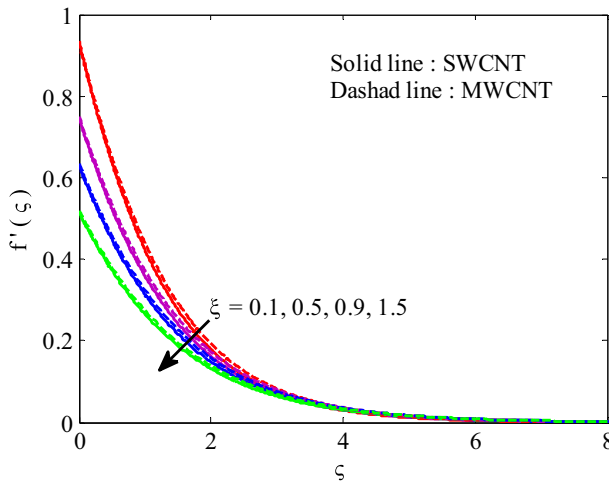
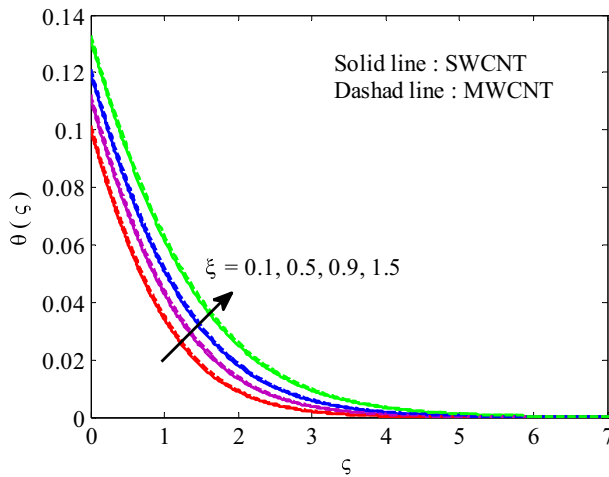**Fig. 6** The MDDIM solutions of dimensionless velocity distribution $f'(\varsigma)$ for different values of ξ

Fig. 7 The MDDIM solutions of dimensionless temperature distribution $\theta(\varsigma)$ for different values of ξ

SWCNT as well as MWCNT nanofluid is declined through, 58% and 77% respectively against the equal class of φ, Nu_x. That means the lessening rate of transfer of heat concerning SWCNT founded nanofluid is more outstanding than MWCNT nanofluid. Furthermore it is ascertained that as φ truly complement by C_{fx} for two kinds of nano particles, merely the opposite result is prevailed against Nu_x. It is observed from Table 3 that, we perceived when Nr changes from 0.0 to 2.0 C_{fx} concerning SWCNT as well as MWCNT founded nanofluid prevails a decrease of 2.97% and 12.8%. Further Nu_x correspondingly declined through 2.8% and 12.68%.

Figures 2 and 3 displayed diagrammatically about the influence of magnetic factor 'M' on temperature also on velocity as well. Magnetic field which acts tangentially over fluid flow resistance creates which named as Lorentz force. The same force makes the fluid slow down like elongating sheet. The velocity profile of fluid reduces but temperature distribution ampli-
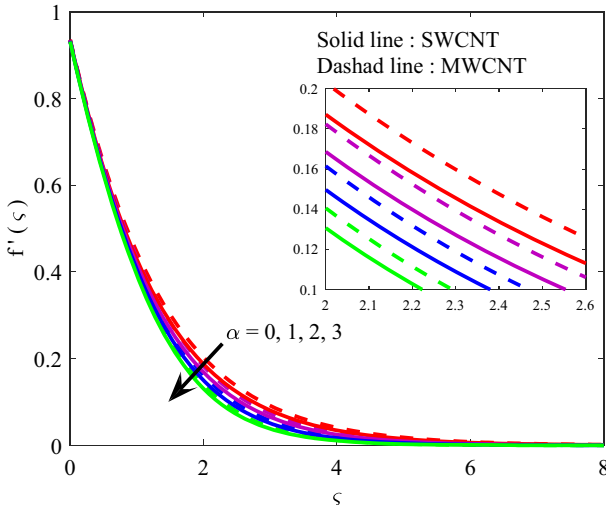
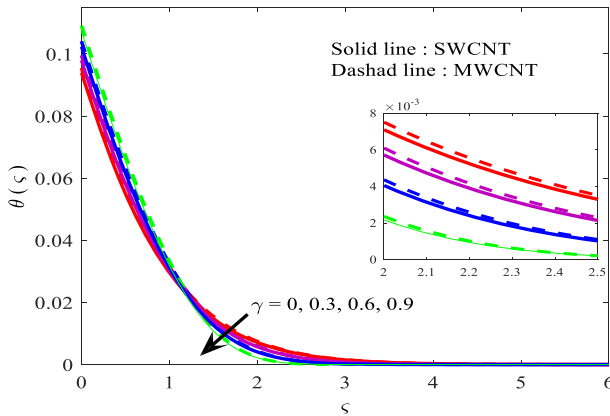**Fig. 8** The MDDIM solutions of dimensionless velocity distribution $f'(\varsigma)$ for different values of $\bar{\alpha}$

Fig. 9 The MDDIM solutions of dimensionless temperature distribution $\theta(\varsigma)$ for different values of γ

fies by enhancing the magnetic factor. Also reveals that the magnetic field acts tangentially, resists transport phenomenon. Out of Fig. 2 it is meritorious that correlated to multi-walled carbon nano tube fluid the swiftness of single walled carbon nano tube disintegrates quickly with M, because of greater density measures for SWCNTs. Even temperature values also grater for MWCNT's wherewith SWCNT's. Principal consideration backside of this is grater thermal conductivity.

Figures 4 and 5 describe about the development of distribution of temperature as well as non-dimensional velocity by using solid nano particle volume proportion χ. Figure 4 designate that besides the progressive measures of φ, velocity profile advances, accordingly the momentum boundary layer increases notably. Also, it's remarkable that MNCNT nanofluid velocity pick up quick development besides SWCNT nano fluid. Figure 5 is manifested by escalating the measures of φ, when the liquids temperature is reduced. Additionally, multi-walled carbon nano tubes have marginally greater values of temperature correlated to carbon
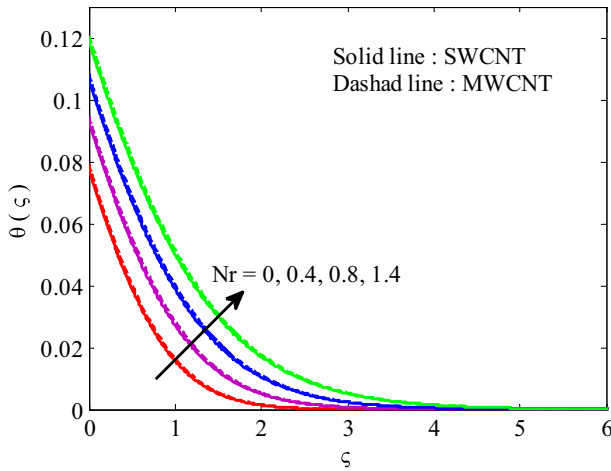
Fig. 10 The MDDIM solutions of dimensionless temperature distribution $\theta(\varsigma)$ for different values of Nr
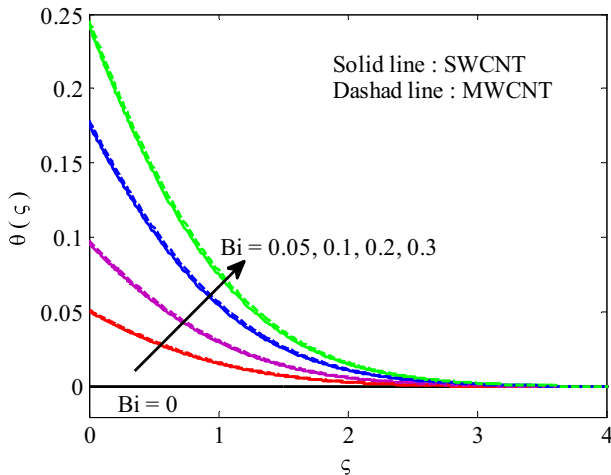

Fig. 11 The MDDIM solutions of dimensionless temperature distribution $\theta(\varsigma)$ for different values of Bi

nano tubes having single walled. As thermal expansion of SWCNTs is lower than MWCNT's which in Table 1 is already examined.

The deviations in temperature and velocity because of proper growth in slip factor are shown in Figs. 6 and 7. Thickness of momentum boundary layer goes down in existence of SWCNT as well as MWCNT together. This prodigy taken place approximately by virtue of actuality such as ξ growth that is true slip increases as a result it accomplishes to a negligible quantity of diffusion by reason of elongated surface of the liquid. Nevertheless, smaller the fluid's momentum, the friction among the layers of fluid and CNTs magnifies, turned out the temperature rises. The same information earlier said was displayed in Fig. 7 clearly.

Figure 8 manifest the influence of relaxation factor $\bar{\alpha}$ of a fluid on velocity profile during SWCNT plus MWCNT nano particles presence. The earlier figure conceals surprising
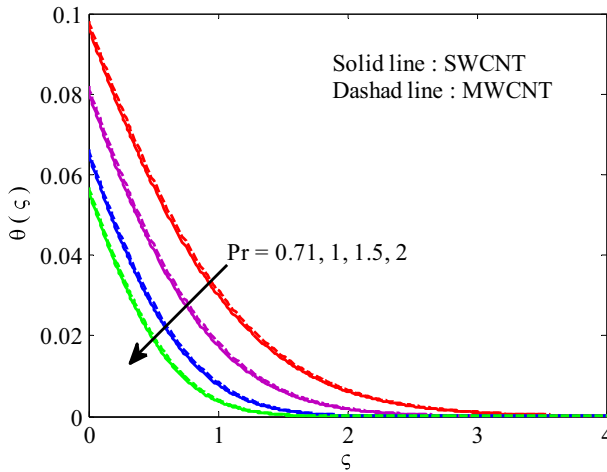
Fig. 12 The MDDIM solutions of dimensionless temperature distribution $\theta(\varsigma)$ for different values of Pr

reflection that, from outward, it explains velocity profile not notably interrupt by $\bar{\alpha}$, if browse carefully means when $\varphi < 1$ it appears the velocity falls.

Aforementioned one occurs as a result of the actuality that $\bar{\alpha}$ illustrate the relaxation time of fluid generally familiar as Deborah number, that performance significant work as an account of viscoelastic materials. When $\bar{\alpha} < 1$ such as the memory duration is lesser then deformation duration α is proportion among the relaxation time and time of deformation. Consequently, the fluid designates as absolutely viscous. If $\bar{\alpha} > 1$, fluid resembles as elastically solid. Hence, base liquid as engine oil that considered as merely viscous in nature. Therefore, we presume $\bar{\alpha} < 1$ as in our study. Like $\bar{\alpha}$ growth, the viscosity amplifies consequently momentum of fluid declines. Hence, in association of CNTs of both types the thickness of momentum boundary layer is falling function of $\bar{\alpha}$.

Figure 9 exhibits the influence of thermal relaxation time (γ) over temperature distribution. Thermal relaxation factor is determined like slow response of heat flux. When $n = 0$ the determined heat flux model, is changed towards Fourier's law. By progressive measures of γ, the thickness of thermal boundary layer goes down and also the rate of reduction is grater for MWCNT nano fluid in both cases. This peculiarity is noticed due to the reality that, SWCNTs thermal conductivity is greater from MWCNTs. Henceforth for SWCNT nano fluid transfer of disintegrate quickly when delay reaction of heat flux amplifies. By multiplying thermal radiation factor Nr, a flourishing in distribution of temperature is detected from Fig. 10 about SWCNT and MWCNT nano fluids as well. Because furtherance in radiation factor inferred reduce in Rosseland radiation absorptive. Therefore, variance of heat flux radiation q_r enhances such that co-efficient of absorption is reduced. Thus, transferred of heat radiation rate of the fluid rises accordingly temperature of fluid grows.

The MDDIM solutions of dimensionless temperature distribution $\theta(\varsigma)$ for different values of Biot number Bi displayed in the Fig. 11. The better convention contributes to the peak surface temperatures that significantly magnifies the temperature and the thicknesses of thermal boundary layer increased.

In Fig. 12 we embellished the fluctuations of temperature beside Prandtl number during both CNTS. Note that, $Pr = 0.7$ is representing the air. We also ascertained that rise in the Prandtl number reduces in the temperature of fluid actually it defines that for greater Prandtl

number thermal boundary layer gets delicate. Prandtl number indicates, momentum distribute as well as thermal distribute ratio. Therefore, Prandtl number utilizes to enhance the cooling rate in convective flows.

Conclusions

In this present article, we analyzed the effects of thermal radiation over CNT-engine oil-based Maxwell-nano fluid with heat flux model by Cattaneo–Christov, through a non-linear elongated surface. SWCNT and MWCNT are considered as nano particles because of their greater thermal conductivity as well as thermal expansion.

Observed points from the current examination are listed below:

1. In the presence of magnetic field velocities as well as temperatures are changed in the opposite manner.
2. Velocity as well as temperature of SWCNT lower than that of MWCNT.
3. For both SWCNT as well as MWCNT on enhancing the values of Nr and Bi temperature raised considerably.
4. The values of skin friction co-efficient, Nusselt number are more concerning MWCNT than those of SWCNTs.

The outcomes demonstrate that the MDDIM is efficient and adequately powerful for use of solving many fluid flow problems. This model contributes advanced characteristics which gives inspiration for further investigations.

References

1. Gupta, A.S.: Hydromagnetic flow past a porous flat plate with Hall effects. Acta Mech. **22**, 281–287 (1975)
2. Hayat, T., Abbas, Z., Asghar, S.: Effects of Hall current and heat transfer on rotating flow of a second-grade fluid through a porous medium. Commun. Nonlinear Sci. Numer. Simul. **13**, 2177–2192 (2018)
3. Saleem, A.M., Aziz, M.A.E.: Effect of Hall currents and chemical reaction on hydro magnetic flow of a stretching vertical surface with internal heat generation/absorption. Appl. Math. Model. **32**, 1236–1254 (2008)
4. Aziz, M.A.E., Nabil, T.: Homotopy analysis solution of hydro magnetic mixed convection flow past an exponentially stretching sheet with Hall current. Math. Probl. Eng. **2012**, 454023 (2012)
5. Pal, D.: Hall current and MHD effects on heat transfer over an unsteady stretching permeable surface with thermal radiation. Comput. Math Appl. **66**(2013), 1161–1180 (2013)
6. Gangadhar, K., Kannan, T., Jayalakshmi, P.: Magnetohydrodynamic micropolar nanofluid past a permeable stretching/shrinking sheet with Newtonian heating. J Braz. Soc. Mech. Sci. Eng. **39**, 4379–4391 (2017)
7. Choi, S.U.S.: Enhancing thermal conductivity of fluids with nanoparticle. In: Siginer, D.A., Wang, H.P. (eds.), Developments and Applications of Non-Newtonian Flows, *ASME FED*, vol 231/MD, 66, pp. 99–105 (1995)
8. Choi, S.U.S., Zhang, Z.G., Yu, W., Lockwood, F.E., Grulke, E.A.: Anomalously thermal conductivity enhancement in nanotube suspensions. Appl. Phys. Lett. **79**, 2252–2254 (2001)
9. Hamilton, R.L., Crosser, O.K.: Thermal conductivity of heterogeneous two component systems. Ind. Eng. Chem. Fundam. **1**, 187–191 (1962)
10. Buongiorno, J.: Convective transport in nano fluids. ASME J. Heat Transf. **128**, 240–250 (2006)
11. Xue, Q.: Model for thermal conductivity of carbon nano tube-based composites. Phys. B **368**, 302–307 (2005)

12. Maxwell, J.C.: Electricity and Magnetism, 3rd edn. Clarendon Press, Oxford (1904)
13. Iijima, S.: Helical microtubules of graphitic carbon. Nature **354**, 56–58 (1991)
14. Endo, M., Hayashi, T., Kim, Y.A., Terrones, M., Dresselhaus, M.S.: Applications of carbon nanotubes in the twenty-first century. Philos. Trans. R. Soc. Lond. A **362**, 2223–2238 (2004)
15. Saito, R., Dresselhaus, G., Dresselhaus, M.S.: Physical Properties of Carbon Nanotubes. Imperial College Press, Singapore (2001)
16. Murshed, S.M., Nieto de Castro, C.A., Lourenco, M.J.V., Lopes, M.L.M., Santos, F.J.V.: A review of boiling and convective heat transfer with nanofluids. Renew. Sustain. Energy Rev. **15**(2011), 2342–2354 (2011)
17. Ganesh Kumar, K., Gireesha, B.J., Manjunatha, S., Rudraswamy, N.G.: Effect of nonlinear thermal radiation on double-diffusive mixed convection boundary layer flow of viscoelastic nano fluid over a stretching sheet. Int. J. Mech. Mater. Eng. **12**, 18 (2017)
18. Khan, U., Ahmed, N., Mohyud-Din, S.T.: Heat transfer effects on carbon nano tubes suspended nano fluid flow in a channel with non-parallel walls under the effect of velocity slip boundary condition: a numerical study. Neural Comput. Appl. **28**, 37–46 (2017)
19. Hayat, T., Ijaz Khan, M., Farooq, M., Alsaedi, A., Waqas, M., Yasmeen, T.: Impact of Cattaneo–Christov heat flux model in flow of variable thermal conductivity fluid over a variable thicked surface. Int. J. Heat Mass Transf. **99**, 702–710 (2016)
20. Hayat, T., Ijaz Khan, M., Farooq, M., Yasmeen, T., Alsaedi, A.: Stagnation point flow with Cattaneo–Christov heat flux and homogeneous–heterogeneous reactions. J. Mol. Liq. **220**, 49–55 (2016)
21. Ijaz Khan, M., Waqas, M., Hayat, T., Alsaedi, A.: A comparative study of Casson fluid with homogeneous–heterogeneous reactions. J. Colloid Interface Sci. **498**, 85–90 (2017)
22. Farooq, M., Ijaz Khan, M., Waqas, M., Hayat, T., Alsaedi, A., Imran Khan, M.: MHD stagnation point flow of viscoelastic nanofluid with non-linear radiation effects. J. Mol. Liq. **221**, 1097–1103 (2016)
23. Hayat, T., Waqas, M., Ijaz Khan, M., Alsaedi, A.: Analysis of thixotropic nanomaterial in a doubly stratified medium considering magnetic field effects. Int. J. Heat Mass Transf. **102**, 1123–1129 (2016)
24. Hayat, T., Ijaz Khan, M., Waqas, M., Alsaedi, A., Farooq, M.: Numerical simulation for melting heat transfer and radiation effects in stagnation point flow of carbon–water nanofluid. Comput. Methods Appl. Mech. Eng. **315**, 1011–1024 (2017)
25. Imran Khan, M., Hayat, T., Ijaz Khan, M., Alsaedi, A.: A modified homogeneous–heterogeneous reactions for MHD stagnation flow with viscous dissipation and Joule heating. Int. J. Heat Mass Transf. **113**, 310–317 (2017)
26. Hayat, T., Ijaz Khan, M., Qayyum, S., Alsaedi, A.: Entropy generation in flow with silver and copper nanoparticles. Colloids Surf. A Physicochem. Eng. Aspects **539**, 335–346 (2018)
27. Hayat, T., Ijaz Khan, M., Farooq, M., Alsaedi, A., Yasmeen, T.: Impact of Marangoni convection in the flow of carbon–water nanofluid with thermal radiation. Int. J. Heat Mass Transf. **106**, 810–815 (2017)
28. Ijaz Khan, M., Hayat, T., Imran Khan, M., Alsaedi, A.: Activation energy impact in nonlinear radiative stagnation point flow of cross nanofluid. Int. Commun. Heat Mass Transf. **91**, 216–224 (2018)
29. Hayat, T., Ijaz Khan, M., Waqas, M., Alsaedi, A.: Mathematical modeling of non-Newtonian fluid with chemical aspects: a new formulation and results by numerical technique. Colloids Surf. A Physicochem. Eng. Aspects **518**, 263–272 (2017)
30. Hayat, T., Ijaz Khan, M., Farooq, M., Alsaedi, A., Imran Khan, M.: Thermally stratified stretching flow with Cattaneo–Christov heat flux. Int. J. Heat Mass Transf. **106**, 289–294 (2017)
31. Qayyum, S., Ijaz Khan, M., Hayat, T., Alsaedi, A.: A framework for nonlinear thermal radiation and homogeneous–heterogeneous reactions flow based on silver–water and copper–water nanoparticles: a numerical model for probable error. Res. Phys. **7**, 1907–1914 (2017)
32. Hayat, T., Qayyum, S., Ijaz Khan, M., Alsaedi, A.: Entropy generation in magnetohydrodynamic radiative flow due to rotating disk in presence of viscous dissipation and Joule heating. Phys. Fluids **30**, 017101 (2018)
33. Hayat, T., Ijaz Khan, M., Waqas, M., Alsaedi, A., Imran Khan, M.: Radiative flow of micropolar nanofluid accounting thermophoresis and Brownian moment. Int. J. Hydrog. Energy **42**, 16821–16833 (2017)
34. Ijaz Khan, M., Waqas, M., Hayat, T., Imran Khan, M., Alsaedi, A.: Behavior of stratification phenomenon in flow of Maxwell nanomaterial with motile gyrotactic microorganisms in the presence of magnetic field. Int. J. Mech. Sci. **131–132**, 426–434 (2017)
35. Imran Khan, M., Ijaz Khan, M., Waqas, M., Hayat, T., Alsaedi, A.: Chemically reactive flow of Maxwell liquid due to variable thicked surface. Int. Commun. Heat Mass Transf. **86**, 231–238 (2017)
36. Ahmed Khan, W.W., Ijaz Khan, M., Hayat, T., Alsaedi, A.: Entropy generation minimization (EGM) of nanofluid flow by a thin moving needle with nonlinear thermal radiation. Phys. B Condens. Matter **534**, 113–119 (2018)

124 Page 24 of 25

Int. J. Appl. Comput. Math (2020) 6:124

37. Hayat, T., Ijaz Khan, M., Qayyum, S., Alsaedi, A., Imran Khan, M.: New thermodynamics of entropy generation minimization with nonlinear thermal radiation and nanomaterials. Phys. Lett. A **382**, 749–760 (2018)

38. Hayat, T., Ahmad, S., Ijaz Khan, M., Alsaedi, A.: Simulation of ferromagnetic nanomaterial flow of Maxwell fluid. Res. Phys. **8**, 34–40 (2018)

39. Dogonchi, A.S., Waqas, M., Ganji, D.D.: Shape effects of copper–oxide (CuO) nanoparticles to determine the heat transfer filled in a partially heated rhombus enclosure: CVFEM approach. Int. Commun. Heat Mass Transf. **107**, 14–23 (2019)

40. Dogonchi, A.S., Waqas, M., Seyyedi, S.M., Tilenooe, M.H., Ganji, D.D.: Numerical simulation for thermal radiation and porous medium characteristics in flow of CuO–H$_2$O nanofluid. J. Braz. Soc. Mech. Sci. Eng. **41**, 249 (2019)

41. Dogonchi, A.S., Chamkha, A.J., Hashemi-Tilehnoee, M., Seyyedi, S.M., Ul-Haq, R., Ganji, D.D.: Effects of homogeneous–heterogeneous reactions and thermal radiation on magneto-hydrodynamic Cu–water nanofluid flow over an expanding flat plate with non-uniform heat source. J. Cent. South Univ. **26**, 1161–1171 (2019)

42. Chamka, A.J., Dogonchi, A.S., Ganji, D.D.: Magneto-hydrodynamic flow and heat transfer of a hybrid nanofluid in a rotating system among two surfaces in the presence of thermal radiation and Joule heating. AIP Adv. **9**, 025103 (2019)

43. Dogonchi, A.S., Armaghani, T., Chamkha, A.J., Ganji, D.D.: Natural convection analysis in a cavity with an inclined elliptical heater subject to shape factor of nanoparticles and magnetic field. Arab. J. Sci. Eng. **44**, 7919–7931 (2019)

44. Dogonchi, A.S., Tayebi, T., Chamkha, A.J., Ganji, D.D.: Natural convection analysis in a square enclosure with a wavy circular heater under magnetic field and nanoparticles. J. Therm. Anal. Calorim. **139**, 661–671 (2020)

45. Dogonchi, A.S., Chamkha, A.J., Seyyedi, S.M., Hashemi-Tilehnoee, M., Ganji, D.D.: Viscous dissipation impact on free convection flow of Cu–water nanofluid in a circular enclosure with porosity considering internal heat source. J. Appl. Comput. Mech. **5**(4), 717–726 (2019)

46. Dogonchi, A.S., Hashim, : Heat transfer by natural convection of Fe$_3$O$_4$–water nanofluid in an annulus between a wavy circular cylinder and a rhombus. Int. J. Heat Mass Transf. **130**, 320–332 (2019)

47. Dogonchi, A.S., Waqas, M., Seyyedi, S.M., Hashemi-Tilehnoee, M., Ganji, D.D.: CVFEM analysis for Fe$_3$O$_4$–H$_2$O nanofluid in an annulus subject to thermal radiation. Int. J. Heat Mass Transf. **132**, 473–483 (2019)

48. Dogonchi, A.S., Hashemi-Tilehnoee, M., Waqas, M., Seyyedi, S.M., Animasaun, I.L., Ganji, D.D.: The influence of different shapes of nanoparticle on Cu–H$_2$O nanofluids in a partially heated irregular wavy enclosure. Phys. A Stat. Mech. Appl. **540**, 123034 (2020)

49. Dogonchi, A.S., Waqas, M., Seyyedi, S.M., Hashemi-Tilehnoee, M., Ganji, D.D.: A modified Fourier approach for analysis of nanofluid heat generation within a semi-circular enclosure subjected to MFD viscosity. Int. Commun. Heat Mass Transf. **111**, 104430 (2020)

50. Mondal, S., Dogonchi, A.S., Tripathi, N., Waqas, M., Seyyedi, S.M., Hashemi-Tilehnoee, M., Ganji, D.D.: A theoretical nanofluid analysis exhibiting hydromagnetics characteristics employing CVFEM. J Braz. Soc. Mech. Sci. Eng. **42**, 19 (2020)

51. Dogonchi, A.S., Waqas, M., Afshar, S.R., Seyyedi, S.M., Hashemi-Tilehnoee, M., Chamka, A.J., Ganji, D.D.: Investigation of magneto-hydrodynamic fluid squeezed between two parallel disks by considering Joule heating, thermal radiation, and adding different nanoparticles. Int. J. Numer. Methods Heat Fluid Flow **30**, 659–680 (2019)

52. Dogonchi, A.S., Waqas, M., Gulzar, M.M., Hashemi-Tilehnoee, M., Seyyedi, S.M., Ganji, D.D.: Simulation of Fe$_3$O$_4$–H$_2$O nanoliquid in a triangular enclosure subjected to Cattaneo–Christov theory of heat conduction. Int. J. Numer. Methods Heat Fluid Flow **29**, 4430–4444 (2019)

53. Dogonchi, A.S., Selimefendigil, F., Ganji, D.D.: Magneto-hydrodynamic natural convection of CuO–water nanofluid in complex shaped enclosure considering various nanoparticle shapes. Int. J. Numer. Methods Heat Fluid Flow **29**, 1663–1679 (2019)

54. Seyyedi, S.M., Dogonchi, A.S., Hashemi-Tilehnoee, M., Asghar, Z., Waqas, M., Ganji, D.D.: A computational framework for natural convective hydromagnetic flow via inclined cavity: an analysis subjected to entropy generation. J. Mol. Liq. **287**, 110863 (2019)

55. Seyyedi, S.M., Dogonchi, A.S., Nuraei, R., Ganji, D.D., Hashemi-Tilehnoee, M.: Numerical analysis of entropy generation of a nanofluid in a semi-annulus porous enclosure with different nanoparticle shapes in the presence of a magnetic field. Eur. Phys. J. Plus **268**, 134 (2019)

56. Seyyedi, S.M., Dogonchi, A.S., Ganji, D.D., Hashemi-Tilehnoee, M.: Entropy generation in a nanofluid-filled semi-annulus cavity by considering the shape of nanoparticles. J. Therm. Anal. Calorim. **138**, 1607–1621 (2019)

57. Seyyedi, S.M., Dogonchi, A.S., Hashemi-Tilehnoee, M., Waqas, M., Ganji, D.D.: Investigation of entropy generation in a square inclined cavity using control volume finite element method with aided quadratic Lagrange interpolation functions. Int. Commun. Heat Mass Transf. **110**, 104398 (2010)
58. Seyyedi, S.M., Dogonchi, A.S., Hashemi-Tilehnoee, M., Waqas, M., Ganji, D.D.: Entropy generation and economic analyses in a nanofluid filled L-shaped enclosure subjected to an oriented magnetic field. Appl. Therm. Eng. (2019). https://doi.org/10.1016/j.applthermaleng.2019.114789
59. Dogonchi, A.S., Ganji, D.D.: Effect of Cattaneo–Christov heat flux on buoyancy MHD nanofluid flow and heat transfer over a stretching sheet in the presence of Joule heating and thermal radiation impacts. Indian J. Phys. **92**, 757–766 (2018)
60. Fourier, J.B.J.: Theorie Analytique De La Chaleur. Chez Firmin Didot, Paris (1822)
61. Cattaneo, C.: Sulla conduzionedelcalore. Atti del Seminario Maermatico e Fisico dell Universita di Modena e Reggio Emilia **3**, 83–101 (1948)
62. Christov, C.I.: On frame indifferent formulation of the Maxwell–Cattaneo model of finite-speed heat conduction. Mech. Res. Commun. **36**(2009), 481–486 (2009)
63. Tibullo, V., Zampoli, V.: A uniqueness result for the Cattaneo–Christove heat conduction model applied to incompressible fluids. Mech. Res. Commun. **38**, 77–99 (2011)
64. Han, S.H., Zheng, L.C., Li, C.R., Zhang, X.X.: Coupled flow and heat transfer in viscoelastic fluid with Cattaneo–Christov heat flux model. Appl. Math. Lett. **38**, 87–93 (2014)
65. Mustafa, M.: Cattaneo–Christove heat flux model for rotating flow and heat transfer of upper convected Maxwell fluid. AIP Adv. (2015). https://doi.org/10.1063/1.4917306
66. Hayat, T., Farooq, M., Alsaedi, A.: Impact of Cattaneo–Christov heat flux in the flow over a stretching sheet with variable thickness. AIP Adv. (2015). https://doi.org/10.1063/1.4929523
67. Hayat, T., Imtiaz, M., Alsaedi, A., Almezal, S.: On Cattaneo–Christovheat flux in MHD flow of Oldroyd-B fluid with homogeneous–heterogeneous reactions. J. Magn. Magn. Mater. **401**, 296–303 (2016)
68. Li, J., Zheng, L., Liu, L.: MHD viscoelastic flow and heat transfer over a vertical stretching sheet with Cattaneo–Christov heat flux effects. J. Mol. Liq. **221**, 19–25 (2016)
69. Oyelakin, I.S., Mondal, S., Sibanda, P.: Cattaneo–Christov nanofluid flow and heat transfer with variable properties over a vertical cone in a porous medium. Int. J. Appl. Comput. Math. **3**, 1019–1034 (2017)
70. Farooq, M., Ahmad, S., Javed, M., Anjum, A.: Analysis of Cattaneo–Christov heat and mass fluxes in the squeezed flow embedded in porous medium with variable mass diffusivity. Res. Phys. **7**, 3788–3796 (2017)
71. Kundu, P.K., Chakraborty, T., Das, K.: Framing the Cattaneo–Christov heat flux phenomena on CNT-based Maxwell nanofluid along stretching sheet with multiple slips. Arab. J. Sci. Eng. **43**, 1177–1188 (2018)
72. Liao, S., Zhao, Y.: On the method of directly defining inverse mapping for nonlinear differential equations. Numer. Algorithms **72**, 989–1020 (2016)
73. Baxter, M., Dewasurendra, M., Vajravelu, K.: A method of directly defining the inverse mapping for solutions of coupled systems of nonlinear differential equations. Numer. Algorithms **77**, 1199–1211 (2018)
74. Dewasurendra, M., Vajravelu, K.: On the method of inverse mapping for solutions of coupled systems of nonlinear differential equations arising in nano fluid flow. Heat Mass Transf. Appl. Math. Nonlinear Sci. **3**, 1–14 (2018)